THE JOURNAL OF PHYSICAL CHEMISTRY B

Article

pubs.acs.org/JPCB

Poisson–Fermi Modeling of the Ion Exchange Mechanism of the Sodium/Calcium Exchanger

Jinn-Liang Liu*

Department of Applied Mathematics, National Hsinchu University of Education, Hsinchu 300, Taiwan

Hann-jeng Hsieh

Department of Applied Mathematics, National Chiao Tung University, Hsinchu 300, Taiwan

Bob Eisenberg*

Department of Molecular Biophysics and Physiology, Rush University, Chicago, Illinois 60612, United States

ABSTRACT: The ion exchange mechanism of the sodium/calcium exchanger (NCX) crystallized by Liao et al. in 2012 is studied using the Poisson–Fermi theory developed by Liu and Eisenberg in 2014. A cycle of binding and unbinding is proposed to account for the Na^+/Ca^{2+} exchange function of the NCX molecule. Outputs of the theory include electric and steric fields of ions with different sizes, correlations of ions of different charges, and polarization of water, along with number densities of ions, water molecules, and interstitial voids. We calculate the electrostatic and steric potentials of the four binding sites in NCX, i.e., three Na^+ binding sites and one Ca^{2+} binding site, with protein charges provided by the software PDB2PQR. The energy profiles of Na^+ and Ca^{2+} ions along their respective Na^+ and Ca^{2+} pathways in experimental conditions enable us to explain the fundamental mechanism of NCX that extrudes intracellular Ca^{2+} across the cell membrane against its chemical gradient by using the downhill gradient of Na^+. Atomic and numerical details of the binding sites are given to illustrate the 3 Na^+:1 Ca^{2+} stoichiometry of NCX. The protein NCX is a catalyst. It does not provide (free) energy for transport. All energy for transport in our model comes from the ions in surrounding baths.

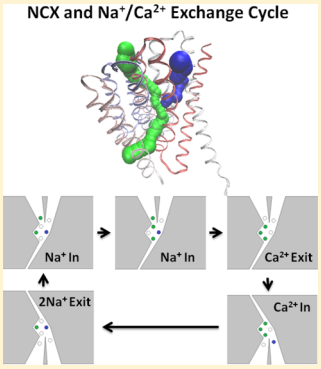

INTRODUCTION

Calcium ions in very low concentrations (10^{-8}–10^{-6} M) control a wide variety of biological functions. The channels, transporters, and binding proteins involved are found in many cells and tissues, where they are essential to vital functions, from contraction of the heart to short-term memory and learning (probably).

A recent review[1] reiterates what has been known for a long time[2,3] and established in more than a thousand investigations: "The Na^+/Ca^{2+} exchanger is the major cardiac extrusion mechanism for the Ca^{2+} that enters via voltage-dependent Ca^{2+} channels with each beat [of the heart]....Ca^{2+} removal by NCX allows myocytes to relax [in conjunction with the sarcoplasmic reticulum]." NCX provides large flows of Ca^{2+} and Na^+ that change direction during normal function. We suspect that NCX directly controls biological functions of great importance in the same sense that the sodium channel controls the speed of the action potential in nerve, but we do not yet know how. Equations are not available that link biological function and the transport properties of the many proteins involved in calcium movements.

In a triumph of modern biology, the molecular basis of the Na^+/Ca^{2+} interactions so striking to Lüttgau and Niedegerke[4] have been revealed, by the cloning of the gene NCX[5] and the determination of the structure of the ancient archaebacterial version NCX_Mj of the Na^+/Ca^{2+} transporter by Liao et al.[6]

The question remains how does NCX work? How does NCX produce the exquisitely tuned coupling of Ca^{2+} and Na^+ studied in such detail in experiments? How does the structure of the molecule use the gradients of concentration of Na^+ and Ca^{2+} and electrical potential to perform its biological function? A structural analysis of NCX cannot itself answer these questions. NCX provides none of the energy for transport. That energy all comes from the gradients of concentration of Na^+ and Ca^{2+} and electrical potential, so a structural analysis that omits those gradients is not sufficient, although it is certainly necessary. The coupling of atomic structure to macroscopic energy sources is the essence of the problem, and thus, atomic and macroscopic theories must be coupled in a multiscale analysis consistent with both atomic and macroscopic physics and conservation laws.

Received: November 25, 2015
Revised: February 23, 2016
Published: February 23, 2016

DOI: 10.1021/acs.jpcb.5b11515
J. Phys. Chem. B 2016, 120, 2658–2669

The question "how does it work?" requires quantitative detail on both atomic and macroscopic scales, because of the complexity of transport in the Na^+/Ca^{2+} system, reproducible in tens of laboratories and hundreds of experimental papers.[2,3] Experiments report numbers in great detail from atomic scale to macroscopic scale in solutions of a variety of contents and concentrations. Understanding how the molecule works means understanding those numbers on both atomic and macroscopic scales. Qualitative reasoning is indispensable but incomplete.

Atomic details of structure control biological function, as is shown in innumerable mutation studies. The actual biological function involves macroscopic variables (like concentration, membrane potential, and flux) that have little meaning on the atomic scale of individual trajectories because averages involve trajectories of some 10^{23} charged atoms with $\sim 10^{15}$ time steps per trajectory, in which all the charges interact through the electric field. Computations of averages of this size present certain numerical difficulties if they are to produce calibrated results, reproducible from one calculation to another, particularly if the macroscopic variables of interest (like the trans-flux across a channel) involve a tiny fraction of all the trajectories. It is not clear that such averages can actually be performed numerically. It is even difficult to define the averages analytically with the precision needed to compute well-defined numerical results. The required stochastic processes involve trajectories with an uncountable number of points moving between surfaces tricky to define with mathematical rigor. Biological function involves ensembles of trajectories and so do the theories, simulations, and experiments that seek to explain that function. The definition and computation of averages of the ensemble is then essential if computations of trajectories are to be compared with experimental and biological results because they too are averages.

Theories and simulations must include relevant atomic details, starting with atomic structures because those details control biological function. They must include macroscopic driving forces because those too control biological functions. Theories and simulations must end with the ensemble properties because they define biological function.

"How does it work?" means how does the atomic scale structure of NCX control transport of Ca^{2+} and Na^+ on a length scale of cells and tissues a million-fold larger than atoms? How does an atomic scale structure control movements of miniscule concentrations of Ca^{2+}?

NCX the transporter is of course all about movements of submicromolar calcium concentrations, so explanations must include those concentrations (and their entropies that form the ideal component of ionic free energy). Atomic scale simulations have intrinsic difficulties in dealing with trace concentrations because they must include 55×10^6 water molecules (55 molar water) for every submicromolar calcium ion. Atomic scale simulations also have difficulty sampling over the macroscopic time scales because atomic motions occur on a 3×10^{-16} second time scale. Precise, unbiased, and converged sampling is needed to be sure entropy is determined accurately enough to deal with experiments measuring macroscopic diffusion. Devices like transporters typically depend on the balance of entropy and energy and dissipation. Each must be computed accurately to be able to estimate the difference on which function depends.

Here we use the Poisson−Fermi model developed in refs 7−12 to analyze the magnificent NCX_Mj structure.[6] We use the power of mathematics and statistical mechanics of Fermi-like distributions to perform the averaging so difficult to do numerically. Of course, the models used by the mathematics do not include all correlations. However, the Poisson−Fermi approach is successful in dealing with properties of gramicidin and L-type calcium channels,[11] and bulk ionic solutions,[12] suggesting that the correlations important in those systems are captured well enough by the present model. After all, this model includes finite size effects, finite size water, and electrical polarization as an output of the model.

In our 2013 paper,[8] we considered water as an implicit medium which fills up the empty voids between spherical ions and derived our first version of the Fermi distribution. We then in the 2014 paper[9] generalized the distribution to include (i) water molecules as spheres and (ii) empty voids between all ions and water molecules. The free energy of any individual particle (ion or water) is determined there by the total distinct configurations of all particles in the entire system in the same mean-field sense used in the Bragg−Williams approach.[13] However, the configuration model of Bragg−Williams is based on the lattice of uniform sites for all ions with equal size (treating water as a continuous medium), whereas that of Fermi distribution is based on the nonuniform lattice of all ions and water treated as spheres of different sizes with interstitial voids between them. The mean-field configurations of nonuniform particles then define a steric (entropic) potential that describes a saturating system. This steric potential resolves the inability of the Boltzmann distribution of point ions and water with zero volumes to deal with the saturation of concentrations produced by the finite size of ions and water. Previous Gibbs free energy functionals based on modified Boltzmann distributions with uniform size spheres or on heuristic formulations have certain difficulties because they give incorrect limits in biologically relevant situations, as we have discussed previously.[9]

The Poisson−Fermi model is consistent with the laws of electrodynamics and thermodynamics. The algebraic approach used here to deal with NCX and its binding sites is a natural extension of the chemical treatment of binding sites. The Poisson−Fermi approach has atomic resolution to deal with the water molecules around Na^+ and Ca^{2+} ions in bulk solution in a calibrated way agreeing with experimental data on activity of Na^+ and Ca^{2+} over a range of salt concentrations.[12] Poisson−Fermi deals with the atomic structure of gramicidin and the ions moving through it in full three-dimensional detail in a range of experimental conditions of salt concentrations and membrane potentials.[11] Poisson−Fermi also deals well with the binding data of the L-type calcium channel over 8 orders of magnitude of concentration of Ca^{2+} using the all spheres representations of previous work[8−10,12] (see the more than 30 papers reviewed in refs 14−16). Our model has been validated with Monte Carlo or molecular dynamics (MD) simulations or experimental data on various simpler systems such as electric double-layer capacitors,[7] single ion activities in bulk solutions,[12] a simplified molecular model of L-type Ca channels,[8−10,12] and gramicidin A channel with full atomic structure.[9,12]

Our approach is a structural analysis of energy. We abstract the permanent charges from all atoms in the NCX_Mj structure and compute the energies (electrostatic, steric, and free energies) of binding ions. We then show how a sequence of binding and unbinding ions can account for the exchange transport in NCX. The algebraic version[10] of the Poisson−Fermi model can compute binding energies from all atomic charges in the structure and from boundary conditions of concentrations of ions. The continuum version[10] of the model

DOI: 10.1021/acs.jpcb.5b11515
J. Phys. Chem. B 2016, 120, 2658−2669

can be used to link the electrical and steric potentials between the bath and the binding site. We show how the gradient of ionic boundary conditions provides all the free energy for transport. Treatments of NCX that do not explicitly include concentrations in the baths cannot account for transport, since NCX is a catalyst and provides none of the energy for transport itself. Indeed, NCX can be viewed as a system of multiple states but one free energy. Perhaps it is useful to view NCX as a "degenerate" system, in the physical sense, a system with multiple conformations but one energy.

Later papers will include specific models of the conformation change of NCX so we can deal with the range of solutions (contents and concentrations) and conditions of such interest to our experimental colleagues (in hundreds of papers on NCX and thousands of papers on transporters). The conformation change involves the profile of charge and the resulting profiles of potentials as much as the profile of mass traditionally identified as "the structure", but it is important to note that the conformation change does not provide any of the (free) energy needed to transport ions. At the end of a transport cycle, NCX has the same free energy as at the beginning. NCX performs its transport function by a complex sequence of binding and unbinding steps similar to that of a two-cycle automobile engine, but the NCX molecule does not have an internal source of energy comparable to the internal combustion of an automobile engine. Any treatment of the function of NCX must include the (free) energy sources for transport, namely, the concentrations and electrical potential of ions in the surrounding macroscopic solutions.

NCX STRUCTURE

The sodium/calcium exchanger (NCX) structure in an outward-facing conformation crystallized by Liao et al.[6] from *Methanococcus jannaschii* (NCX_Mj with the PDB code 3v5u)[17] is shown in Figure 1A. The NCX consists of 10 transmembrane (TM) helices in which eight helices (TMs 2 to 5 and 7 to 10 labeled numerically in the figure) form in the center a tightly packed core that consists of four cation binding sites arranged in a diamond shape and shown as three green spheres (denoted by S_{ext}, S_{mid}, and S_{int}) and one blue sphere (S_{Ca}) in Figure 1B. The number written between any two adjacent spheres in Figure 1B (and in Figure 2) denotes the distance between the centers of the spheres in angstroms (Å).

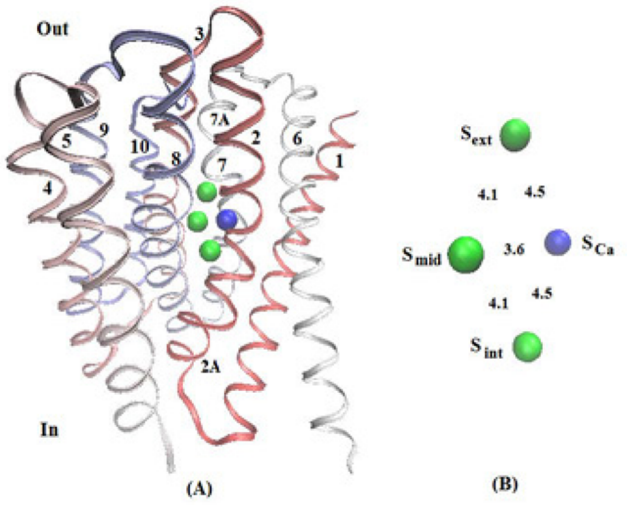

Figure 1. Structure of NCX_Mj. (A) Viewed from the membrane, the four binding sites shown as four spheres are tightly formed by 8 transmembrane helices labeled by 2 to 5 and 7 to 10. (B) The three green and one blue spheres illustrate three putative Na^+ binding sites (denoted by S_{ext}, S_{mid}, and S_{int}) and one Ca^{2+} site (S_{Ca}), respectively. The number written between any two adjacent spheres indicates the distance of the two sites in angstroms.

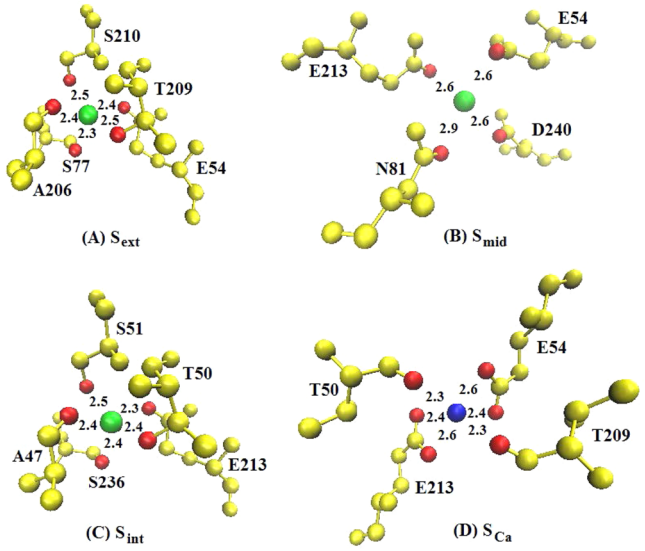

Figure 2. Na^+ and Ca^{2+} ions in the binding sites S_{ext} (A), S_{mid} (B), S_{int} (C), and S_{Ca} (D) are chelated by 4 Ser (S210, S77, S51, S236), 2 Thr (T209, T50), 2 Glu (E54, E213), 2 Ala (A206, A47), 1 Asp (D 240), and 1 Asn (N81) amino acid residues in which the charged oxgens are shown in red spheres. The number written between any two spheres indicates their distance in angstroms.

The Na^+ and Ca^{2+} ions are chelated by 4 Ser (S210, S77, S51, S236), 2 Thr (T209, T50), 2 Glu (E54, E213), 2 Ala (A206, A47), 1 Asp (D 240), and 1 Asn (N81) amino acid residues, as shown in Figure 2, where the red spheres denote the charged oxygens in these residues. Some of the charged oxygens are shared by several bound ions. The total number and total charge of these oxygens are 12 and $-6.36e$, respectively, where e denotes the proton charge and the partial charges on the oxygens were obtained by the software PDB2PQR.[18] The conversion of spatial coordinates of a PDB file to a structure with specific distributions of charge is a crucial part of the modeling process explained in detail in PDB2PQR and its supporting publications. In a very real sense, our model starts with the output of the PDB2PQR software, as much as it starts with the PDB coordinates that are output of Liao et al.'s work.[6]

The total charges around S_{ext}, S_{mid}, S_{int}, and S_{Ca} are -2.63, -2.2, -2.63, and $-3.3e$, respectively. These charges play a crucial role in our analysis of the exchange mechanism of NCX. The total number of atoms in the whole NCX protein is $N = 4591$ with the total positive and total negative charges being 385.185 and $-382.185e$, respectively. All charges in the NCX are included in our model. Ionized glutamates form the "bidentate" binding site for Ca^{2+} discovered and discussed at length by Liao et al.[6] We assume that all glutamates are fully charged. Protonated glutamates can be easily computed in our model if experimental evidence should suggest that they are relevant.

We use two methods, namely, the VMD software[19] and the molecular surface generation (MSG) method described in ref 7,

DOI: 10.1021/acs.jpcb.5b11515
J. Phys. Chem. B 2016, 120, 2658−2669

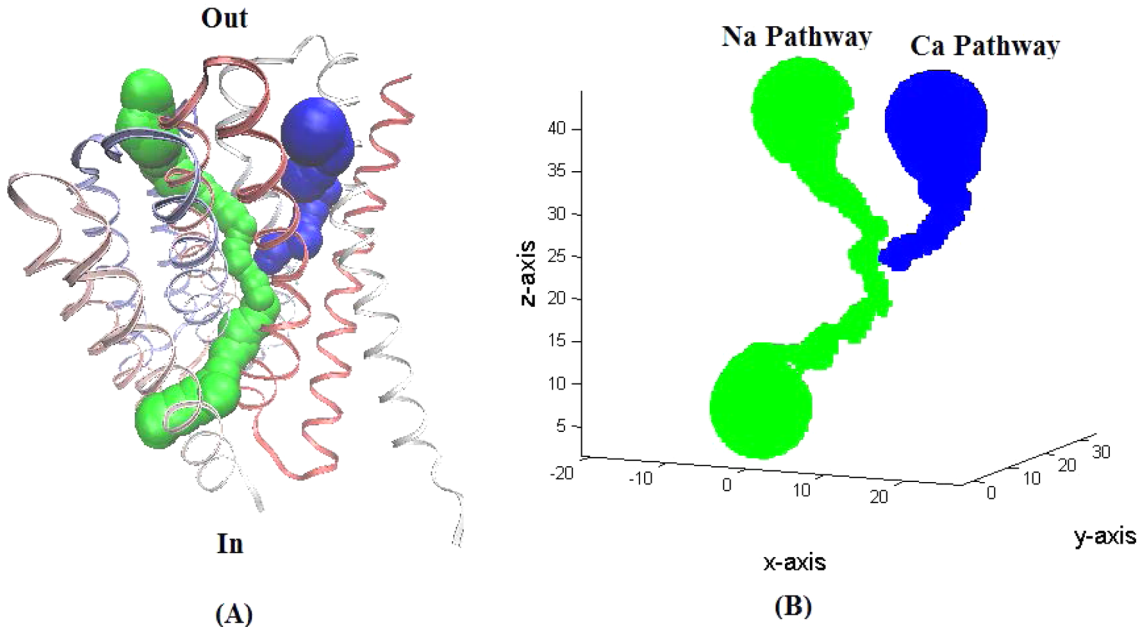

Figure 3. 3D Na^+ and Ca^{2+} pathways in NCX explored by (A) the VMD software[19] and (B) the molecular surface generation method in ref 7 and shown in green and blue, respectively.

to explore the geometry of Na^+ and Ca^{2+} passageways in detail, as shown in Figure 3A and B, respectively, where the Na^+ and Ca^{2+} passageways are drawn in green and blue, respectively. The molecular surface generation is important because it describes the geometry of our NCX machine just as the macroscopic surface of an engine describes its geometry. Understanding an engine would be inconceivable without a precise statement of where the piston ends and the cylinder begins. Understanding NCX function depends on similar structural detail, in our opinion.

The surface-rendering method implemented in the VMD software[19] is used to explore the pathways starting from the location of a binding ion at S_{ext}, S_{int}, or S_{Ca} (in Figure 1A and B) and then all the way up (or down) to the pathway mouth by cross-sectional slicing along the channel axis. The locations of the four binding ions in Figure 2 are given in the PDB file of NCX. The sectional size is 0.5 Å, the channel axis is determined one by one at each cross section, and the radius of the channel pore at each cross section is determined manually by inserting a variable sphere in the VMD rendering graphics.

The Na^+ and Ca^{2+} pathways were surprisingly convoluted and winding compared to what we expected from the structures of other channels such as gramicidin,[20] potassium,[21] sodium,[22] and transient receptor potential[23] channels. The zigzag structure made finding and defining the pores a difficult task. Our analysis does not show an obvious biological role or reason for the tortuosity. Perhaps a later analysis including flux and current will be more revealing. The pore radii of Na^+ and Ca^{2+} pathways calculated by the MSG method with a mesh size of 0.5 Å in discretization[7] are shown in green and blue curves in Figure 4 with respect to the z coordinate that runs along their respective channel axes. The z coordinates of the four binding sites S_{ext}, S_{mid}, S_{int}, and S_{Ca} are 25.945, 22.724, 20.166, and 23.467 Å, respectively.

We assume that water is not present in the diamond-shaped binding pocket (Figure 1A and B). This assumption is based on the structural study in ref 6 that the binding sites S_{ext}, S_{mid}, and S_{int} can accommodate three Na^+ ions (as shown in Figure 5 in

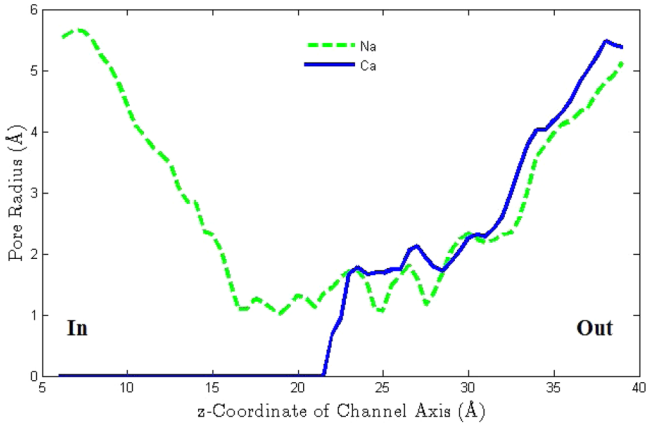

Figure 4. Pore radii of Na^+ and Ca^{2+} pathways are shown in green and blue curves, respectively, with respect to the z coordinate along their respective channel axes.

ref 6) during the ion-exchange reaction, and the hydrophobic patch on the conserved Pro residues extends from the Ca^{2+} binding site S_{Ca} to the Ca^{2+} pathway (Figure 4C in ref 6). The assumption is supported by Figure 4 according to our calculations, where the radii of the two entrances of the binding pocket in the Na^+ pathway are about 1.1 Å. Water (with a radius of 1.4 Å) is too large to enter the binding pocket via this pathway. The crystal structure of NCX_Mj[6] appears to be rigid in the present work, but it is not. The flexibility (and correlations) of the structure is described quantitatively (but of course approximately and in a model dependent way) by the entropy of the Poisson–Fermi model. Of course, the radius 1.1 Å in Figure 4 obtained by our method is subject to numerical errors that may make this assumption questionable. This assumption should be carefully studied in future work.

THEORY

The Poisson–Fermi theory proposed in refs 8 and 9 is used to study the binding mechanism and stoichiometry of NCX using

DOI: 10.1021/acs.jpcb.5b11515
J. Phys. Chem. B 2016, 120, 2658–2669

the atomic structure of NCX. Ours is an atomic theory just as are simulations of molecular dynamics. We use mathematics to average microscopic trajectories to a macroscopic reduced model that includes many but not all correlations. Up to now, fully atomic simulations have not been able to deal with the trace concentrations of calcium and the time scales involved in the biological function and experimentation on NCX.

The outward facing structure of Figures 1A, 3A, and 3B is directly resolved in the structure of Liao et al.[6] The inward facing structure has not yet been seen in X-ray, but Liao et al.[6] have proposed a structure, a kind of intramolecular homology model. Most creatively, they have simply swapped TMs 6−7A and TMs 1−2A helices to create an inwardly facing structure of NCX_Mj. The corresponding Ca^{2+} pathway is then inverted to an inward-facing configuration in their model shown in Figure 5. The outward and inward conformations can rapidly

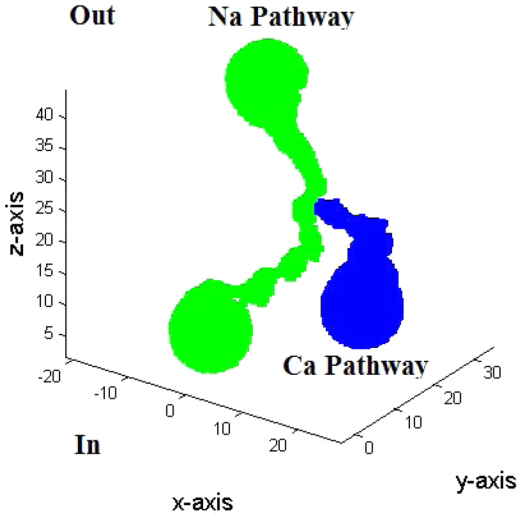

Figure 5. An inward-facing 3D model of Na^+ and Ca^{2+} pathways in NCX.

interchange and hence facilitate the rapid ion exchange reaction in NCX by a simple sliding motion of the gating bundle (TMs 1, 2A, 6, and 7A) hinged at the bends in the structure between TMs 2A and 2B and TMs 7A and 7B.[6,24]

Both outward- and inward-facing Ca^{2+} pathways shown in Figures 3B and 5 will be used to calculate the electrostatic potentials in and near the four binding sites S_{ext}, S_{mid}, S_{int}, and S_{Ca}. In later work, we will try to understand the change between these two conformations. In addition to the four binding sites, we consider four extra sites near the binding pocket, as shown in Figure 6A and B for outward- and inward-facing conformations, respectively, where aS1, aS5, aS6, and aS8 are the extra sites and bS2 = S_{ext}, bS3 = S_{mid}, bS4 = S_{ext}, and bS7 = S_{Ca} are the binding sites. The sites aS1, bS2, bS3, bS4, and aS5 in green are located in the Na^+ pathway, whereas aS6, bS7, and aS8 in blue are in the Ca^{2+} pathway. These sites are numbered by assuming reaction paths in which Na^+ ions move inward (without changing direction, i.e., always with forward motion) from extracellular to intracellular and Ca^{2+} ions move outward from intracellular to extracellular bath without changing direction.

Extra sites (aS1, aS5, aS6, and aS8) are determined empirically and close to entrance or exit locations of the binding pocket. Each extra site is centered at the channel axis of its pathway. The distance between aS1 (aS5) and bS2 (bS4) is comparable to that between bS2 and bS3. The distance between aS8 (aS6) and bS7 is comparable to that between aS1 and bS3. The energy profiles at all 8 sites can be used to describe the desired forward motion of Na^+ and Ca^{2+} ions. The extra sites are henceforth called access sites (aS1, aS5, aS6, and aS8) to separate them from the binding sites (bS2, bS3, bS4, and bS7) for which the coordinates are determined by the NCX structure, as shown in Figure 2. All of these coordinates are fixed throughout this paper. Electrical potentials in the pathways will be determined with various combinations of Na^+ and Ca^{2+} ions occupying the access and binding sites.

Algebraic Model. In refs 9 and 10, we proposed an algebraic model for calculating the electric potential ϕ_b in a binding site Ω_b by applying Coulomb's law to the individual atoms of the protein structure, and bound ions. This model was able to calculate the binding curve of the calcium channel from 10^{-10} to 10^{-2} M Ca^{2+} ions (in the presence of 32 mM Na^+ ions) with only a handful of parameters, never adjusted once chosen. Our model computes electrostatic and steric potentials expected from all the charges in the structure of NCX_Mj. Figures 1, 2, and 6 show the atomic structures of NCX analyzed this way. In these figures, b denotes the site aS1, bS2, ..., or aS8.

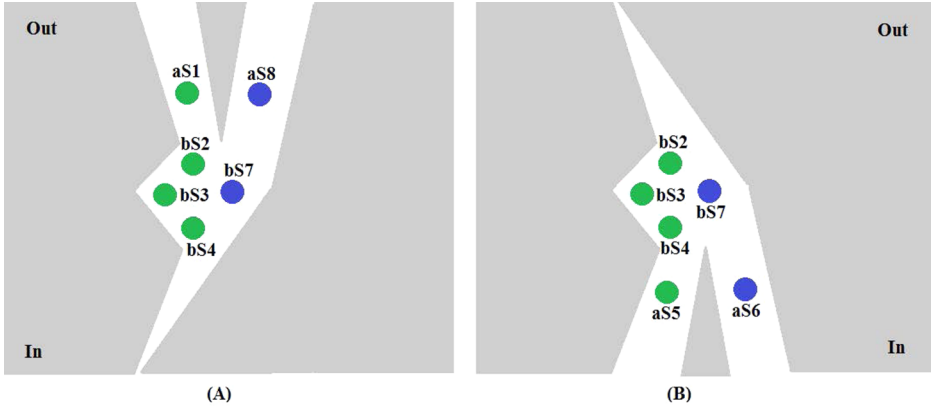

Figure 6. In (A) outward-facing structure and (B) inward-facing homology conformations, the eight sites aS1, bS2, ..., aS8 marked in green and blue disks located in the Na^+ (green) and Ca^{2+} (blue) pathways, respectively, are used for electrostatic analysis, where bS2 = S_{ext}, bS3 = S_{mid}, bS4 = S_{ext}, and bS7 = S_{Ca} are binding sites and aS1, aS5, aS6, and aS8 are access sites to the binding sites (binding pocket).

DOI: 10.1021/acs.jpcb.5b11515
J. Phys. Chem. B 2016, 120, 2658−2669

The electric potential in Ω_b at b = bS7, for example, is calculated by

$$\phi_b = \frac{1}{4\pi\epsilon_0}\left(\frac{1}{6}\sum_{k=1}^{6}\left(\sum_{j=1}^{N}\frac{q_j}{\epsilon_p|c_j - A_k|} + \sum_{m=1,m\neq \mathrm{bS7}}^{8}\frac{O_m^b q_m}{\epsilon_b|c_m - A_k|}\right) + \frac{O^b_{Ca^{2+}} q_{Ca^{2+}}}{\epsilon_b a_{Ca^{2+}}}\right) \quad (1)$$

where the occupancy number is $O^b_{Ca^{2+}} = 1$ if Ω_b is occupied by a Ca^{2+} and $O^b_{Ca^{2+}} = 0$ if it is unoccupied, ϵ_0 is the vacuum permittivity, q_j is the charge of the jth atom in the NCX protein with N atoms, c_j is the center of that atom, A_k is one of six surface points on the spherical Ca^{2+} ion, as shown in Figure 7,

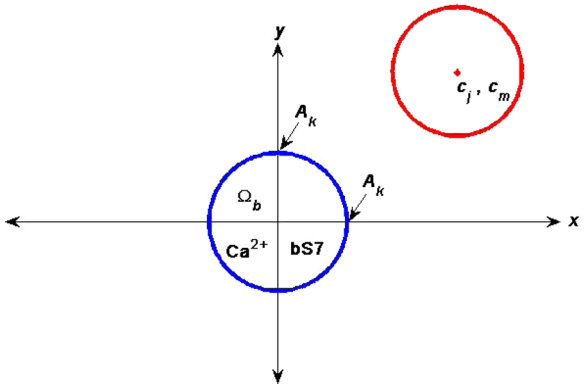

Figure 7. For eq 1, the domain Ω_b of the binding site bS7 occupied by a Ca^{2+} is illustrated by the blue circle, where A_k denotes one of six surface points on the spherical Ca^{2+} ion. Any atom in NCX located at c_j or any other m = aS1, bS2, ..., aS6 or aS8 site centered at c_m is illustrated by the red circle.

$|c_j - A_k|$ is the distance between c_j and A_k, q_m denotes the charge of any other site m = aS1, bS2, ..., aS6 or aS8 if $O^b_m \neq 0$, ϵ_p is a dielectric constant for the NCX protein domain, ϵ_b is a dielectric constant for all Ω_b with b = aS1, bS2, ..., aS8, and $a_{Ca^{2+}}$ is the radius of Ca^{2+}.

We can also use the algebraic approach to compute the steric potential. The steric potential measures the effect of crowding of ions and side chains. It depends on the bath concentrations C_i^B of all ionic species i = 1, ..., K and water (denoted by the K + 1 species) in the solvent domain Ω_s. If $O^b_{Ca^{2+}} = 1$, the steric potential (entropy) of the bound ion Ca^{2+} at b = bS7 depends on its local environment characterized by an unknown volume v_b of Ω_b and its global bath condition by a constant void fraction $\Gamma^B = 1 - \sum_{j=1}^{K+1} v_i C_i^B$, where v_i is the volume of a species i particle (hard sphere). The steric potential S_b^{trc} and the unknown volume v_b can be obtained by solving the following two equations (with $O^b_{Ca^{2+}} = 1$)

$$O^b_{Ca^{2+}} = v_b C^B_{Ca^{2+}} \exp(-\beta_{Ca^{2+}}\phi_b + S_b^{trc}) \quad (2)$$

$$S_b^{trc} = \ln\frac{1 - \sum_{j=1}^{m} v_j/V_{sites}}{\Gamma^B} \quad (3)$$

where V_{sites} = 104.81 Å^3 is the volume of the site region shown in Figure 6A or B, m is the total number of the sites in Figure 6A or B occupied by Na^+ or Ca^{2+} ions, and v_j is the volume of the ion at the jth site. The site region in Figure 6A or B consists of two access sites, four binding sites, and the empty space between any two sites in the Na^+ or Ca^{2+} pathway. These two equations are derived from the Fermi-like distribution[9]

$$C_i(\mathbf{r}) = C_i^B \exp(-\beta_i\phi(\mathbf{r}) + S^{trc}(\mathbf{r})), \quad S^{trc}(\mathbf{r}) = \ln\frac{\Gamma(\mathbf{r})}{\Gamma^B},$$
$$\Gamma(\mathbf{r}) = 1 - \sum_{i=1}^{K+1} v_i C_i(\mathbf{r}) \quad (4)$$

where $C_i(\mathbf{r})$ is a concentration function of spatial variable $\mathbf{r}$ in Ω_s, $\phi(\mathbf{r})$ is an electrostatic potential function, $S^{trc}(\mathbf{r})$ is a steric potential function, $\Gamma(\mathbf{r})$ is a void fraction function, $\beta_i = q_i/(k_BT)$, q_i is the ionic charge, k_B is the Boltzmann constant, and T is an absolute temperature.

The distribution eq 4 is of Fermi type, since all concentration functions can saturate. The concentration functions are bounded from above, i.e., $C_i(\mathbf{r}) < 1/v_i$ for all particle species with any arbitrary (or even infinite) potential $\phi(\mathbf{r})$ at any location $\mathbf{r}$ in Ω_s.[9] We suppose that the Fermi-like distribution contains sufficient detail to deal with the correlations of crowded ions because it succeeds in bulk solutions[12] and in calcium channels.[11]

The potential function is $\phi(\mathbf{r}) = \phi_b$ in Ω_b but is still undetermined in the region $\Omega_s\backslash(\cup\Omega_b)$, namely, the solvent domain Ω_s excluding the union set $\cup\Omega_b$ of all binding domains Ω_b for b = aS1, bS2, ..., aS8. It can be obtained by solving the Poisson−Fermi (PF) equation[7,8,25]

$$\epsilon_w\epsilon_0(l_c^2\nabla^2 - 1)\nabla^2\phi(\mathbf{r}) = \sum_{i=1}^{K} q_i C_i(\mathbf{r}) = \rho(\mathbf{r}),$$
$$\forall \mathbf{r} \in \Omega_s\backslash(\cup\Omega_b) \quad (5)$$

with suitable boundary conditions, where ϵ_w is the dielectric constant of bulk water and $\rho(\mathbf{r})$ is a charge density function. These boundary conditions link the binding site to the electric potential in the baths, providing the electrical component of the driving force for ion transport through NCX. If the correlation length is $l_c \neq 0$, the dielectric operator $\epsilon_w\epsilon_0(1 - l_c^2\nabla^2)$ approximates the permittivity of the bulk solvent and the linear response of correlated ions and yields a dielectric function $\hat{\epsilon}(\mathbf{r})$ as an output from eq 5.[8] Moreover, the polarization of water can be described as an output of the PF equation by means of a polarization charge density.[8] For more details about the model (mathematical, physical, and chemical aspects), we refer to refs 7−12.

Since ions and water are treated as hard spheres with interstitial voids, the Poisson−Fermi model can compute the electrical and steric energies from the physical parameters of all atoms. For the electrical potential in eq 1, the total number of protein atoms N = 4591 with the coordinates c_j are provided by the Protein Data Bank.[17] The radii and charges q_j of these atoms are given by the software PDB2PQR.[18] The maximum number of ions in the binding pocket in eq 1 is 8. For the steric potential in eq 3, the individual volumes v_j of ions and the total volume V_{sites} of the binding pocket are calculated using the ionic radii given in Table 1 and the channel radii shown in Figure 4. Therefore, the Poisson−Fermi model computes electrical and steric potentials from all atoms in the NCX protein and all ions in the binding pocket while keeping electrolyte solutions in the rest of the channel pore domain and in the extra- and intracellular baths as a continuum dielectric medium with variable permittivity. The coordinates of atoms and ions are all kept fixed throughout the solution process

DOI: 10.1021/acs.jpcb.5b11515
J. Phys. Chem. B 2016, 120, 2658−2669

Table 1. Values of Model Notations

symbol	meaning	value	unit
k_B	Boltzmann constant	1.38×10^{-23}	J/K
T	temperature	298.15	K
e	proton charge	1.602×10^{-19}	C
ϵ_0	permittivity of vacuum	8.85×10^{-14}	F/cm
ϵ_b, ϵ_p, ϵ_w, ϵ_m	dielectric constants	10, 20, 78.45, 2	
$l_c = 2a_i$	correlation length	$i = Na^+, Ca^{2+}$	Å
a_{Na^+}, $a_{Ca^{2+}}$	radii	0.95, 0.99	Å
a_{Cl^-}, a_{H_2O}	radii	1.81, 1.4	Å
O_m^b	site occupancy	0 or 1	
$[Na^+]_o$, $[Na^+]_i$	bath concentrations[6]	120, 60	mM
$[Ca^{2+}]_o$, $[Ca^{2+}]_i$	bath concentrations[6]	1, 33	μM
i, o	intra, extracellular		

because the Poisson−Fermi model can only describe a steady-state equilibrium system.

NCX Structure and Continuum Model. Here we use the Poisson−Fermi model to analyze binding sites of NCX. In a very real sense, our paper is a quantitative complement to the structural work of Liao et al. A quantitative complement is needed because a structural model cannot in itself deal with the energetics of catalysis. The energy for transport comes from the baths, and the structural analysis must be extended in a multiscale manner to include the macroscopic properties of the baths. Our model is a first step in that extension from atomic structure to biological function.

RESULTS

Since the Fermi distribution eq 4 includes the steric potential, the total energy of an ion i at a location $\mathbf{r}$ is expressed as

$$E_i(\mathbf{r}) = -k_B T(-\beta_i \phi(\mathbf{r}) + S^{trc}(\mathbf{r})) = q_i \phi(\mathbf{r}) - S^{trc}(\mathbf{r}) k_B T \quad (6)$$

We define the total potential (electric and steric potentials) at a site b as

$$\Psi_b = (q_b \phi_b - S_b^{trc} k_B T)/q_b \quad (7)$$

with the unit $k_B T/e$, where ϕ_b is calculated by eq 1, S_b^{trc} is obtained by eq 3, and $q_b = q_{Na^+}$ for b = aS1, bS2, ..., aS5 and $q_b = q_{Ca^{2+}}$ for b = aS6, bS7, aS8. This is a definition of an energy landscape that involves occupied and unoccupied sites. A total potential state (TPS) of these sites is said to be stable if all Ψ_b are negative. For example, TPS1 and TPS4 in Figure 8 are stable, whereas TPS2, TPS3, and TPS5 are unstable, as shown by the blue bars on the right panels in Figure 8, where each bar denotes the value of Ψ_b. The site notations aS1, bS2, ..., aS8 in Figure 6A and B are also shown in the panels of TPS1 and TPS2. The green (or blue) dot in Figure 8 indicates that the corresponding site is occupied by a Na^+ (or Ca^{2+}) ion.

Numerical values of the model symbols used in the calculation are given in Table 1 with two salts NaCl and $CaCl_2$ in both extra- and intracellular baths. The dielectric constant is an empirical parameter in the standard Poisson equation as well as in our Coulomb potential, eq 1. We choose the dielectric constants $\epsilon_b = 10$ and $\epsilon_p = 20$ in the protein and binding domains, respectively, because the electrical potential at the binding site b = bS7 in eq 1 is screened more (with larger $\epsilon_p = 20$) by the larger number of and farther protein atoms (N = 4591) than by the fewer and closer 8 or less bound ions (smaller $\epsilon_b = 10$).

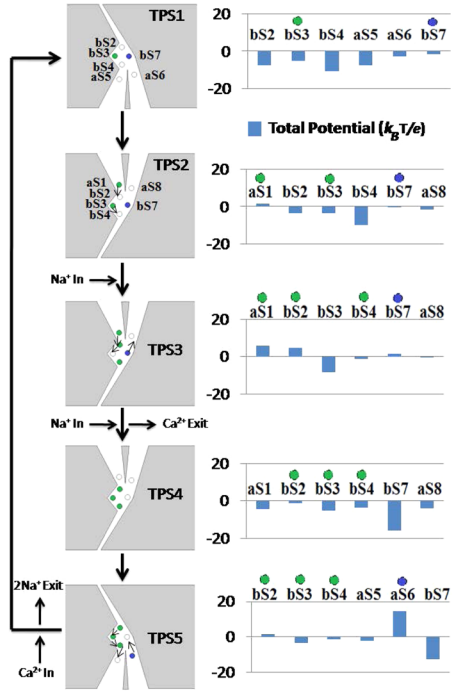

Figure 8. Schematic diagram of a cycle of Na^+/Ca^{2+} exchange in NCX, which consists of five total potential states (TPS) where TPS1 and TPS4 are stable and TPS2, TPS3, and TPS5 are unstable. Two Na^+ and one Ca^{2+} ions enter the binding pocket (bS2, bS3, bS4, bS7) in the outward- (TPS2, TPS3, TPS4) and inward-facing (TPS1, TPS5) conformations, respectively. The magnitude of the electrical potential (in $k_B T/e$) at each site aS1, bS2, ..., aS8 for TPS is shown by a blue bar. The green and blue dots in the diagram represent Na^+ and Ca^{2+} ions occupying the respective sites.

Proposed Mechanism and Transport Cycle. The states TPS1 to TPS5 in Figure 8 can now be used to describe the ion exchange mechanism of NCX. The ion exchange mechanism we propose involves a sequence of state changes driven by the electrical and steric forces, involving the bath concentrations and electrical potentials. The cycle is a kind of biological reciprocating engine, in which combustion is replaced by binding and piston motion is replaced by ionic electro-diffusion in gradients of electrical and steric potential. The complexity and detail of the model is a barrier to understanding by both readers and authors, but the complexity and detail is that necessary to describe any reciprocating engine, whether in an automobile or in life, that performs its function by moving from one state to another, with different structures and energies.

TPS1. This TPS is in the inward-facing configuration in Liao et al.'s homology model, where one Na^+ is at bS3 (denoted by Na^+_{bS3}) and one Ca^{2+} is at bS7 (Ca^{2+}_{bS7}), as shown in green and blue dots, respectively, in the top left two panels of Figure 8. The total potentials at these two sites are $\Psi_{bS3}^{TPS1} = -5.03$ and $\Psi_{bS7}^{TPS1} = -1.38$ $k_B T/e$ (the unit $k_B T/e$ will be omitted in what follows). It is important to remember that the potentials here and in the following paragraphs are computed outputs of the model of Liao et al. using the physics of our Poisson−Fermi treatment. The potentials can be viewed as a quantitative estimate of the qualitative binding seen in the structure and homology model, using perhaps the simplest consistent treatment of electrostatics and excluded volume effects. Consistent means that neither the electrostatic energies nor the excluded volume energies are assumed. These energies are

DOI: 10.1021/acs.jpcb.5b11515
J. Phys. Chem. B 2016, 120, 2658−2669

always computed from the structure and the Poisson−Fermi formulas.

Stability Analysis of Proposed Cyclic Mechanism. The potentials at bS2 to bS7 are all negative, meaning that the ions Na^+_{bS3} and Ca^{2+}_{bS7} will be stable at their respective sites and will not move to other sites; i.e., the total energy of each ion is not sufficiently large to overcome its binding energy (total potential energy). We assume that the conformational change from inward-facing (TPS1) to outward-facing (TPS2) is activated by the binding Ca^{2+} ion at bS7 or by some other unknown mechanism that we hope some day to understand, even discover. After the conformational change, a Na^+ ion from the extracellular bath can access aS1 because the potential well $\Psi^{TPS1}_{bS2} = -7.68$ at the unoccupied site bS2 is deep enough to attract Na^+ ions if the extracellular concentration $[Na^+]_o$ is sufficiently large. By the Fermi distribution eq 4, the selectivity ratio of Na^+ to Ca^{2+} by NCX from the extracellular bath to the binding site bS2 is defined and given as

$$\frac{C_{Na^+}(\mathbf{r})}{C_{Ca^{2+}}(\mathbf{r})} = \frac{[Na^+]_o \exp(-q_{Na^+}\Psi^{TPS1}_{bS2})}{[Ca^{2+}]_o \exp(-q_{Ca^{2+}}\Psi^{TPS1}_{bS2})} = \frac{120\cdot 1000}{2164} = 55.4 \quad (8)$$

under the experimental[6] bath conditions $[Na^+]_o$ and $[Ca^{2+}]_o$ given in Table 1. In our model, the driving force for Ca^{2+} extrusion is determined by the total potential $\Psi^{TPS1}_{bS7} = -1.38$, which is quite shallow (small). This indeed agrees with the small driving force for Ca^{2+} extrusion observed in experiments.[26]

TPS2. Once aS1 is occupied by a Na^+ (Na^+_{aS1}), we obtain $\Psi^{TPS2}_{aS1} = 1.94$ and $\Psi^{TPS2}_{bS2} = -3.74$.

Instability Analysis of Proposed Cyclic Mechanism. The potential Ψ^{TPS2}_{aS1} is positive, making Na^+_{aS1} unstable. Na^+_{aS1} should then move from aS1 to bS2 because Ψ^{TPS2}_{bS2} is negative (note this is after aS1 was previously occupied by a Na^+) and thus attracts the positive ion Na^+_{aS1}. When Na^+_{aS1} moves to bS2, the potential of Na^+_{bS3} at bS3 changes from $\Psi^{TPS2}_{bS3} = -3.52$ (stable) to $\Psi_{bS3} = 3.1$. This new potential is very positive, unstable, and we do not show it here. Hence Na^+_{bS3} should move from bS3 to bS4 because $\Psi^{TPS2}_{bS4} = -10.08$ is very attractive. During these Na^+ movements, the potential of the Ca^{2+} ion at bS7 changes from $\Psi^{TPS1}_{bS7} = -1.38$ in TPS1 to $\Psi^{TPS2}_{bS7} = -0.02$ in TPS2.

TPS3. Meanwhile, another Na^+ ion (Na^+_{aS1}) may access aS1 provided that $[Na^+]_o$ is sufficiently large. Three Na^+ ions in this TPS can produce a large electric force on the Ca^{2+}_{bS7} ion at bS7 (with $\Psi^{TPS3}_{bS7} = 1.65$) and consequently repel it from bS7 to aS8 ($\Psi^{TPS3}_{aS8} = -0.54$). The ions Na^+_{aS1} ($\Psi^{TPS3}_{aS1} = 6.07$), Na^+_{bS2} ($\Psi^{TPS3}_{bS2} = 4.77$), and Ca^{2+}_{bS7} ($\Psi^{TPS3}_{bS7} = 1.65$) are all unstable (with positive potential) and therefore should proceed forward. From the energy profile of $\Psi^{TPS3}_{aS1} = 6.07$, $\Psi^{TPS3}_{bS2} = 4.77$, and $\Psi^{TPS3}_{bS3} = -8.89$ in TPS3, we observe that the driving force—the potential difference of Ψ^{TPS3}_{bS3} and Ψ^{TPS3}_{aS1}—is $\Delta\Psi = \Psi^{TPS3}_{bS3} - \Psi^{TPS3}_{aS1} = -14.96$, which is very large in magnitude, implying that the ions Na^+_{aS1}, Na^+_{bS2}, and Ca^{2+}_{bS7} move very rapidly. NCX can thus efficiently perform Ca^{2+} and Na^+ homeostasis in cells. The energy producing this driving force comes from the downhill gradient of Na^+ ions[6,26]—the difference between the extracellular $[Na^+]_o = 120$ mM and intracellular $[Na^+]_i = 60$ mM in Table 1—and from the selectivity of Na^+ ions from the extracellular bath to the binding site bS2 by eq 8. Note that the extracellular and intracellular baths are connected by the Na^+ pathway in both conformations, as shown in Figures 3 and 5.

TPS4. After the rapid movement of the unstable ions Na^+_{aS1}, Na^+_{bS2}, and Ca^{2+}_{bS7} in TPS3, the ions Na^+_{aS1} and Na^+_{bS2} settle into their respective sites Na^+_{bS2} ($\Psi^{TPS4}_{bS2} = -1.05$) and Na^+_{bS3} ($\Psi^{TPS4}_{bS3} = -5.21$). The total potential of the ion Na^+_{bS4} at bS4 changes from $\Psi^{TPS3}_{bS4} = -1.07$ in TPS3 to $\Psi^{TPS4}_{bS4} = -3.6$ in TPS4. Therefore, Na^+_{bS2}, Na^+_{bS3}, and Na^+_{bS4} are all stable in TPS4. By the time these three ions settle stably in respective sites, their combined force has already repelled Ca^{2+}_{bS7} away from the binding pocket because $\Psi_{bS7} = 1.71$ (not shown) or $\Psi_{aS8} = 3.43$ (not shown) if it would stay at bS7 or aS8. Both $\Psi_{bS7} = 1.71$ and $\Psi_{aS8} = 3.43$ are positive, implying that the Ca^{2+} ion is unstable when Na^+_{bS2}, Na^+_{bS3}, and Na^+_{bS4} are in the binding pocket so the Ca^{2+} ion should exit the binding pocket. TPS1 and TPS4 are the only two stable states in the cycle in Figure 8.

We assume that a conformational change from outward-facing (TPS4) to inward-facing (TPS5) is activated by the loss of Ca^{2+} ion at bS7 = S_{Ca} ($\Psi^{TPS4}_{bS7} = -16.02$) or by some other unknown mechanism. Note that the electric potential $\Psi^{TPS4}_{bS7} = -16.02$ at the unoccupied site bS7 is the largest in magnitude not only at all 8 sites and in all 5 TPS but also in the entire NCX structure: S_{Ca} is charged with the largest amount ($-3.3e$) of negative charges from the amino acid residues of NCX (see Figure 2D). This large potential seems likely to play a key role in the unknown mechanism of the conformational change.

TPS5. After the assumed conformational change, the highly charged and unoccupied site bS7 ($\Psi^{TPS4}_{bS7} = -16.02$) is exposed to the cytosol that can provide a Ca^{2+} ion to access aS6. The selectivity ratio of Ca^{2+} to Na^+ by NCX from the intracellular bath to the binding site bS7 is remarkably large

$$\frac{C_{Ca^{2+}}(\mathbf{r})}{C_{Na^+}(\mathbf{r})} = \frac{[Ca^{2+}]_i \exp(-q_{Ca^{2+}}\Psi^{TPS4}_{bS7})}{[Na^+]_i \exp(-q_{Na^+}\Psi^{TPS4}_{bS7})} = \frac{33\cdot 9065622}{60\cdot 1000} = 4986.1 \quad (9)$$

in the intracellular bath conditions $[Ca^{2+}]_i = 33\ \mu M$ and $[Na^+]_i = 60$ mM in Table 1. Note that the extracellular and intracellular baths are not connected by the Ca^{2+} pathway (see Figure 5). When a Ca^{2+} ion is at aS6 in TPS5, it is extremely unstable and should proceed because $\Psi^{TPS5}_{aS6} = 14.51$ is the largest positive value in Figure 8. The potential force driving this Ca^{2+} ion from aS6 to bS7 is $\Delta\Psi = \Psi^{TPS5}_{bS7} - \Psi^{TPS5}_{aS6} = -12.78 - 14.51 = -27.29$, which is extremely large in magnitude, implying that the Ca^{2+} ion moves very rapidly. Moreover, when the Ca^{2+} ion is at aS6, Na^+_{bS2} ($\Psi^{TPS5}_{bS2} = 1.6$) becomes unstable and Na^+_{bS3} ($\Psi^{TPS5}_{bS3} = -3.15$) and Na^+_{bS4} ($\Psi^{TPS5}_{bS4} = -1.73$) become less stable compared with $\Psi^{TPS4}_{bS3} = -5.21$ and $\Psi^{TPS4}_{bS4} = -3.6$ in TPS4. By the time the Ca^{2+}_{aS6} ion reaches the stable site bS7 in TPS1, only one Na^+ ion is stable at bS3, as shown in TPS1. This implies that two Na^+ ions in TPS5 have been repelled out of the binding pocket by the electric forces of the divalent Ca^{2+}_{bS7} and the monovalent Na^+_{bS3} in TPS1. This completes a cycle of Na^+/Ca^{2+} exchange.

In the above description, Na^+ and Ca^{2+} ions move in opposite directions in NCX. When two Na^+ ions enter and one Ca^{2+} ion exits the binding pocket, the stable TPS1 is followed by the unstable TPS2 and TPS3. When one Ca^{2+} ion enters and two Na^+ ions exit the binding pocket, the stable TPS4 is

DOI: 10.1021/acs.jpcb.5b11515
J. Phys. Chem. B 2016, 120, 2658−2669

followed by the unstable TPS5. The stable state is destabilized by the entry of an ion into the pocket. The entry of ions into the pocket is determined by the extracellular and intracellular bath conditions $[Ca^{2+}]_{i,o}$ and $[Na^+]_{i,o}$.

Mechanism of Coupling. A great deal of attention has been focused on the mechanism by which sodium drives calcium movement, i.e., by which the gradient of sodium electrochemical potential is coupled to the movement of calcium so calcium can move against its own gradient of electrochemical potential.

In our model, the movements of ions are driven by the instability of the (total) potential for the ion/binding complex. The potential is a combination of electrical and steric potentials and is a quantitative output of the calculations of Poisson−Fermi theory applied to the structure of Liao et al. It is not assumed. Thus, the energetics of coupling is determined by the energetics of the instability of the binding site/ion complex. The energy that produces the instability comes from the downhill gradient of Na^+ bath concentrations ($[Na^+]_o - [Na^+]_i$) and the selectivity ratio eq 8 of Na^+ to Ca^{2+} in TPS2 and TPS3 and from the intracellular Ca^{2+} bath concentration ($[Ca^{2+}]_i$) and the selectivity ratio eq 9 of Ca^{2+} to Na^+ in TPS5. Of course, this discussion of binding is not a quantitative prediction of NCX function. That requires an actual calculation of fluxes in a variety of conditions. And it involves details of the conformation change and how it limits (or does not limit) flux. We will turn to those issues in later papers.

For TPS4, there is no room for water in between S_{ext} (bS2), S_{mid} (bS3), and S_{int} (bS4) according to the binding structure shown in Figures 1B and 2, and water cannot occupy the hydrophobic S_{Ca} (bS7). If a water molecule were in the binding pocket, we could not obtain the main result of the NCX exchange mechanism in Figure 8 because the water molecule would occupy one of the four binding sites bS2, bS3, bS4, and bS7, which would result in completely different TPS1−TPS5. Our energetic analysis in Figure 8 again supports the assumption that water is not present in the binding pocket.

Stoichiometry. There are 2 Na^+ and 1 Ca^{2+} ions entering and exiting the binding pocket during a single cycle, as shown in Figure 8. There are 3 states (TPS2, TPS3, TPS4) and 2 states (TPS1, TPS5) for 2 Na^+ ions and 1 Ca^{2+} ion entering the binding pocket, respectively. Assuming that the total time T of an exchange cycle is equally shared by the 5 TPS, the stoichiometry of NCX in transporting Na^+ and Ca^{2+} ions can then be inferred from our model as

$$\frac{3}{5}\mathrm{T}\cdot 2\mathrm{Na}^+ : \frac{2}{5}\mathrm{T}\cdot 1\mathrm{Ca}^{2+} = 3\mathrm{Na}^+ : 1\mathrm{Ca}^{2+} \tag{10}$$

which agrees with the generally accepted stoichiometry (see reviews of Blaustein and Lederer[2] and Dipolo and Beaugé[3]) since the pivotal work of Reeves and Hale[27] and other subsequent experimental results.[28−31]

The energy levels of stable TPS1 and TPS4 in Figure 8 are not sensitive to the variation of locations of the extra sites, whereas those of unstable TPS2, TPS3, and TPS5 are sensitive. However, it can be easily inferred from TPS5, for example, and numerically verified that slight variations of the location of the extra site aS6 for the coming Ca^{2+} will not change the instability of TPS5; i.e., the exchange cycle in Figure 8 is not sensitive to slight variations of the locations of access sites.

It is essential to describe movements of ions in TPS1 to TPS5 along the energy profiles given in Figure 8, which consequently imply the stoichiometry eq 10. In chemistry, movement along a reaction path is a widely used (and valuable) method of creating a reduced model of a reaction involving myriads of atomic trajectories. In channel modeling, the classical rate theory[32] with energy profiles is a heuristic tool for describing movements of ions through a channel pore. Our description of the exchange mechanism in Figure 8 is a heuristic application of that theory. The Poisson−Fermi model is not a kinetic model but a steady-state model that yields energy levels of ions at equilibrium. The time T in eq 10 is also heuristic as frequently used in the rate theory. Kinetic models will be developed in our future work to verify this heuristic assumption. Nevertheless, the present work may serve as an important step toward more comprehensive simulations of ion transport in NCX for which the literature is very scarce. From our analysis in Figure 8, we conjecture that NCX spends 3/5 and 2/5 of its cyclic time in upward and downward conformations, respectively, during ion exchange transportation. This prediction may be valuable as well for future MD or continuum simulations on the conformational change mechanism in NCX.

All numerical results so far have been obtained by the algebraic eqs 1−3 that include the potential in the binding pocket but do not include the potential in the baths. The next question is how to extend the potential function $\phi(\mathbf{r})$ from the binding pocket with various ϕ_b in Ω_b for b = aS1, bS2, ..., aS8 to extracellular and intracellular baths—from few ions to numerous particles. The solvent domain Ω_s consists of the baths and Na^+ and Ca^{2+} pathways (Figure 3B or Figure 5). We use the Poisson−Fermi eq 5 to calculate the potential function $\phi(\mathbf{r})$ in $\Omega_s\backslash(\cup\Omega_b)$ for TPS3 in the outward-facing Y pathway configuration (Figure 3B). We also compute the steric function $S^{\mathrm{trc}}(\mathbf{r})$ and the concentration functions $C_i(\mathbf{r})$ by eq 4. Numerical methods for solving $\phi(\mathbf{r})$ by the PF equation with ϕ_b as a Dirichlet boundary in each Ω_b and with the protein charges in the biomolecular domain Ω_m are described in detail in refs 7 and 11. For TPS1 (with the inverted Y shape inward facing, from the homology model), TPS2 (Y shape), TPS4 (Y shape), and TPS5 (inverted Y shape), the numerical results can be obtained in a similar way. Therefore, we only present the results for the case of TPS3. A cross section of the 3D simulation domain $\Omega = \Omega_s \cup \Omega_m$ is shown in Figure 9, where the solvent domain Ω_s consists of extracellular and intracellular baths (in white) and Na^+ (green) and Ca^{2+} (blue) pathways and the biomolecular domain Ω_m (yellow) consists of the cell membrane and NCX protein.

The electric potential profiles for TPS3 along the channel axes of Na^+ and Ca^{2+} pathways are shown by the green and blue curves in Figure 10, respectively. Each profile was obtained by averaging the values of $\phi(\mathbf{r})$ at each cross section along the axis of the solvent domain (including baths), where $\phi(\mathbf{r})$ was calculated by eq 1 in Ω_b and by eq 5 in $\Omega_s\backslash(\cup\Omega_b)$. The counterions of the three Na^+ and one Ca^{2+} ions fixed at their respective sites in TPS3 are included in the total charge density $\rho(\mathbf{r})$ in eq 5. The counterions are in the domain $\Omega_s\backslash(\cup\Omega_b)$, while the fixed ions are in the binding domain $\cup\Omega_b$.

The notations aS1, bS2, bS3, bS4, bS7, and aS8 in the figure correspond to the potentials Ψ_b given in eq 7 for TPS3. The continuous potential profile in the Na^+ pathway (green curve) shows that the Na^+ ion at aS1 is unstable and should move to bS3 (left, in) because the potential at bS3 is very negative. Similarly, the blue curve illustrates a continuous profile for the Ca^{2+} ion at bS7 which should move to the right (out) because the potentials at aS8 and aS9 are more negative. These two

DOI: 10.1021/acs.jpcb.5b11515
J. Phys. Chem. B 2016, 120, 2658−2669

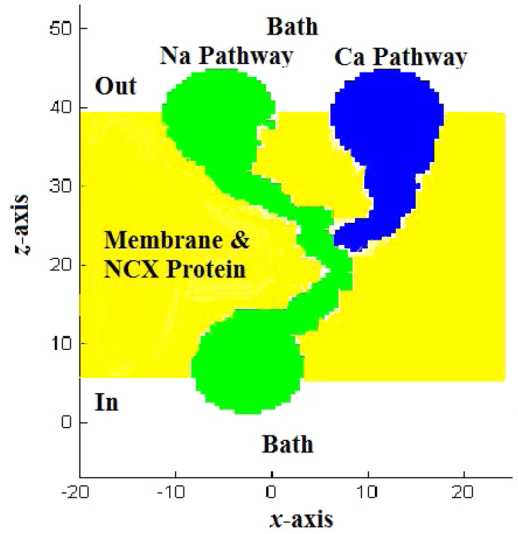

Figure 9. A cross section of 3D simulation domain $\Omega = \Omega_s \cup \Omega_m$, where the solvent domain Ω_s consists of extracellular and intracellular baths (in white) and Na^+ (green) and Ca^{2+} (blue) pathways and the biomolecular domain Ω_m (yellow) consists of cell membrane and NCX protein.

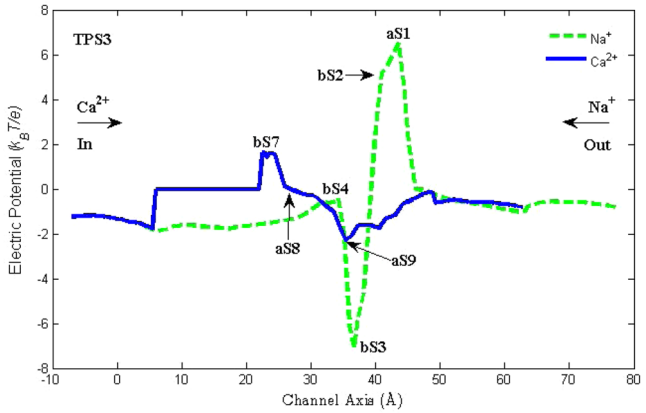

Figure 10. Electric potential profiles of $\phi(\mathbf{r})$ along the axes of Na^+ and Ca^{2+} pathways are shown in green and blue curves, respectively. Each curve was obtained by averaging the values of $\phi(\mathbf{r})$ at cross sections along the axis of the solvent domain Ω_s that contains both two baths and a pathway. The notations aS1, bS2, bS3, bS4, bS7, and aS8 indicate the potential values obtained by eq 1 for EPS3, as shown in Figure 8. The potential at aS9 was obtained by eq 5, not eq 1. The potential profiles suggest opposite flows of Na^+ and Ca^{2+} ions, as illustrated in the figure. The same averaging method was used for Figures 11 and 12.

curves represent the electrostatic potential $\phi(\mathbf{r})$ of all ions in the entire solvent domain Ω_s and all charges in the NCX protein domain Ω_m with distinguishable energy hills and valleys at access and binding sites, where the hills are the locations of the ions occupying their respective sites in TPS3. The electric potential at the valley site aS9 shown in Figure 10 is −2.22 and was calculated using eq 5 because the site is not in the union set $\cup\Omega_b$ of the eight access and binding sites.

Multiscale Electrostatics. Our numerical methods are multiscale,[11] since both Poisson's theory of continuous charges in eq 5 and Coulomb's law of discrete charges in eq 1 are used to obtain the potential function $\phi(\mathbf{r})$ in the entire solvent domain Ω_s. The potential function $\phi(\mathbf{r})$ in the biomolecular domain Ω_m is obtained from the structure by using the Poisson equation

$$-\epsilon_m\epsilon_0\nabla^2\phi(\mathbf{r}) = \sum_{j=1}^{N} q_j\delta(\mathbf{r}-\mathbf{r}_j), \quad \forall \mathbf{r}\in\Omega_m \tag{11}$$

where ϵ_m is the dielectric constant of biomolecules, q_j is the charge of the jth atom in the NCX protein with N atoms, and $\delta(\mathbf{r}-\mathbf{r}_j)$ is the Dirac delta function at $\mathbf{r}_j$.[7] The singular δ functions and the potential function $\phi(\mathbf{r})$ across two different domains Ω_s and Ω_m are treated by the simplified matched interface and boundary method.[7] Note that the z coordinates of bS4 = S_{mid} and bS7 = S_{Ca} are 22.724 and 23.467, respectively, as shown in Figure 1B. The distance between bS4 and bS7 in Figure 10 is about 10 Å because the winding Na^+ and Ca^{2+} pathways elongate differently along two channel axes that are measured from the same z coordinate at $z = -7$ in the figure.

The dielectric function $\hat{\epsilon}(\mathbf{r})$ resulting from eq 5 is not relevant to the total potential energies given in Figure 8, the main result of this work, since those energies were calculated by the algebraic eqs 1−3 with fixed dielectric constants $\epsilon_b = 10$ and $\epsilon_p = 20$ in the protein and binding domains, respectively. It is however relevant to the continuous electric potential profiles in Figure 10, since it is a continuous function varying from its bath value $\epsilon_w = 80$ to the binding value $\epsilon_b = 10$ in the solvent domain $\Omega_s\backslash(\cup\Omega_b)$. The dielectric function profile (not shown) is an output of solving the algebraic model in $\cup\Omega_b$, the fourth-order Poisson−Fermi eq 5 in $\Omega_s\backslash(\cup\Omega_b)$, and the standard second-order Poisson eq 11 in Ω_m. Details of numerical methods are given in refs 7 and 11.

Entropic Interactions. The Poisson−Fermi model can also describe the steric (entropic) interactions between all particles in the system. The void fraction function $\Gamma(\mathbf{r})$ in eq 4 is a mean-field description of how much void is present in a unit volume at any location $\mathbf{r}\in\Omega_s$. The bath void fraction Γ^B is constant when the bath concentrations C_i^B of all ions and water are fixed. The bath void fraction has nothing to do with the channel or channel protein. The other void function describes the channel. $\Gamma(\mathbf{r})$ depends on all concentration functions $C_i(\mathbf{r}) = C_i^B \exp(-\beta_i\phi(\mathbf{r}) + S^{trc}(\mathbf{r}))$ that in turn depend self-consistently on the electric and steric potential functions $\phi(\mathbf{r})$ and $S^{trc}(\mathbf{r})$ as well as on the bath conditions C_i^B. Therefore, the steric potential S_b^{trc} of bound ions in the binding pocket calculated by eq 3 is linked to the bath void fraction Γ^B via the steric potential function $S^{trc}(\mathbf{r})$ in the PF equation just as the binding potential ϕ_b linked to bath potentials by $\phi(\mathbf{r})$.

Figure 11 shows that the site region with the volume V_{sites} = 104.81 Å^3 (see Figure 6A and B) has more voids than the bath does because $S^{trc}(\mathbf{r}) = \ln\frac{\Gamma(\mathbf{r})}{\Gamma^B} = 0.45$ in Figure 11, i.e., $\Gamma(\mathbf{r}) > \Gamma^B$. However, the concentration of a single Na^+ ion at aS1 in TPS3 is $C_{Na^+}(\mathbf{r}) = O^b_{Na^+}/v_b$ = 224.17 M (with $O^b_{Na^+} = 1$ and v_b = 3.59 Å^3), as shown in Figure 12, which is extremely large when compared with the outer bath concentration of Na^+ ions $C^B_{Na^+} = [Na^+]_o$ = 120 mM. Two hundred molar, as concentrated as it is, is still much less than the saturation value of the Fermi distribution $C^{max}_{Na^+} = 1/v_{Na^+}$ = 462.39 M (that fills the volume entirely), as asserted by our theory. The average concentration of 3 Na^+ and 1 Ca^{2+} ions in the binding pocket and access sites in TPS3 is reduced to 63.41 M because the enlarged volume V_{sites} = 104.81 Å^3 contains unoccupied sites and empty spaces between sites. The magnitude of 63.41 M is more than 500 times the bath concentration 120 mM because of the highly

DOI: 10.1021/acs.jpcb.5b11515
J. Phys. Chem. B 2016, 120, 2658−2669

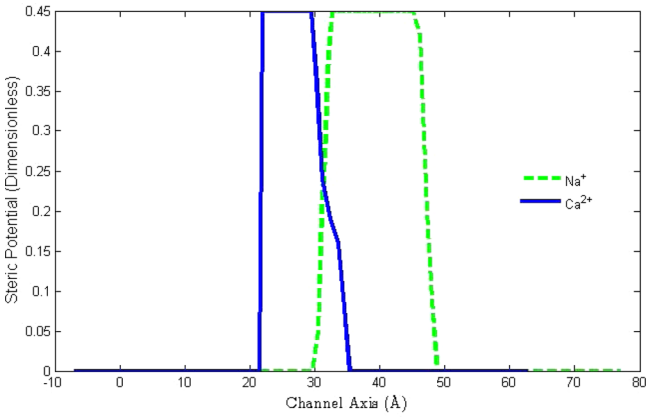

Figure 11. Steric potential profiles of $S^{trc}(\mathbf{r})$ are shown in green and blue curves, respectively.

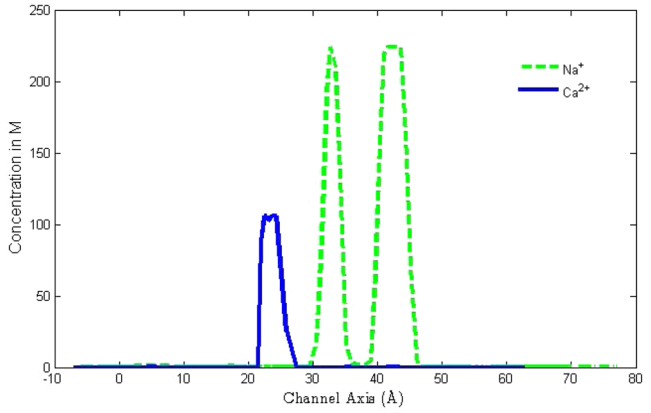

Figure 12. Concentration profiles of $C_{Na^+}(\mathbf{r})$ and $C_{Ca^{2+}}(\mathbf{r})$ are shown in green and blue curves, respectively.

charged binding sites (see Figure 2). The binding sites are indeed very crowded in terms of ionic concentrations.

CONCLUSION

Using the NCX_Mj structure and the Poisson−Fermi theory, we propose a 5-TPS (total potential state) cyclic model of the sodium/calcium exchange mechanism in NCX. This cyclic model can describe the $3Na^+$:$1Ca^{2+}$ stoichiometry of NCX. Each TPS characterizes an energy profile of ions from baths to binding sites in that state. The energy profiles determine ionic motions in NCX. Structures are determinants of the electric and steric fields but are not sources of energy: NCX is an enzyme, a catalyst. We show explicitly that our model of NCX does not use energy beyond ion gradients and electric and steric fields with sources in the baths and not in the catalytic protein NCX itself, as described consistently by the Poisson−Fermi theory. The energy that produces ionic motions comes from the downhill gradients of Na^+ and/or Ca^{2+} concentrations between extracellular and intracellular baths. The Poisson−Fermi theory can describe energetic end points and selectivity of NCX, although a kinetic model of conformational changes remains outside its grasp. That model is not known at present, but we do know that it will involve the energetics of ions in the baths, the structure and conformations of the NCX and its binding sites, and the way the protein catalyzes the movement of ions without providing energy of its own. The model will be multivalued in the mathematical sense, and degenerate in the physical sense, since the NCX enzyme must enter and leave the transport reaction cycle with the same free energy. NCX has one and the same free energy at entry and at exit, even as it accelerates the motions of ions that would have occurred eventually (according to thermodynamics) in the absence of the protein.

AUTHOR INFORMATION

Corresponding Authors

*E-mail: jinnliu@mail.nhcue.edu.tw.
*E-mail: beisenbe@rush.edu.

Notes

The authors declare no competing financial interest.

ACKNOWLEDGMENTS

This work was supported in part by the Ministry of Science and Technology, Taiwan (under Grant No. MOST 103-2115-M-134-004-MY2), to J.-L.L. and by the Mathematical Biosciences Institute (MBI) of the Ohio State University, USA (under the MBI Long Term Visitor Program) to J.-L.L. and B.E. We thank De-Sian He and Shao-Hong Chen for their computational help on this work. We (J.-L.L. and B.E.) are grateful to the MBI, particularly to its director Marty Golubitsky and Guowei Wei, the head of the Mathematical Molecular Biosciences Program. They provided the resources that allowed us to live and work side by side for two months in 2015. They also continue to provide motivation, and scientific inspiration, just as important as finance.

REFERENCES

(1) Shattock, M. J.; Ottolia, M.; Bers, D. M.; Blaustein, M. P.; Boguslavskyi, A.; Bossuyt, J.; Bridge, J. H. B.; Chen-Izu, Y.; Clancy, C. E.; Edwards, A.; et al. Na^+/Ca^{2+} Exchange and Na^+/K^+-ATPase inthe Heart. *J. Physiol.* **2015**, *593*, 1361−1382.
(2) Blaustein, M. P.; Lederer, W. J. Sodium/Calcium Exchange: Its Physiological Implications. *Physiol. Rev.* **1999**, *79*, 763−854.
(3) Dipolo, R.; Beaugé, L. Sodium/Calcium Exchanger: Influence of Metabolic Regulation on Ion Carrier Interactions. *Physiol. Rev.* **2006**, *86*, 155−203.
(4) Lüttgau, H.-C.; Niedergerke, R. The Antagonism between Ca and Na Ions on the Frog's Heart. *J. Physiol.* **1958**, *143*, 486−505.
(5) Nicoll, D. A.; Longoni, S.; Philipson, K. D. Molecular Cloning and Functional Expression of the Cardiac Sarcolemmal Na(+)-Ca2+Exchanger. *Science* **1990**, *250*, 562−565.
(6) Liao, J.; Li, H.; Zeng, W.; Sauer, D. B.; Belmares, R.; Jiang, Y. Structural Insight into the Ion-Exchange Mechanism of the Sodium/Calcium Exchanger. *Science* **2012**, *335*, 686−690.
(7) Liu, J.-L. Numerical Methods for the Poisson-Fermi Equation in Electrolytes. *J. Comput. Phys.* **2013**, *247*, 88−99.
(8) Liu, J.-L.; Eisenberg, B. Correlated Ions in a Calcium Channel Model: a Poisson-Fermi Theory. *J. Phys. Chem. B* **2013**, *117*, 12051−12058.
(9) Liu, J.-L.; Eisenberg, B. Poisson-Nernst-Planck-Fermi Theory for Modeling Biological Ion Channels. *J. Chem. Phys.* **2014**, *141*, 22D532.
(10) Liu, J.-L.; Eisenberg, B. Analytical Models of Calcium Binding in a Calcium Channel. *J. Chem. Phys.* **2014**, *141*, 075102.
(11) Liu, J.-L.; Eisenberg, B. Numerical Methods for a Poisson-Nernst-Planck-Fermi Model of Biological Ion Channels. *Phys.Rev. E* **2015**, *92*, 012711.
(12) Liu, J.-L.; Eisenberg, B. Poisson-Fermi Model of Single Ion Activities in Aqueous Solutions. *Chem. Phys. Lett.* **2015**, *637*, 1−6.
(13) Scheutjens, J. M. H. M.; Fleer, G. J. Statistical Theory of the Adsorption of Interacting Chain Molecules. 1. Partition Function, Segment Density Distribution, and Adsorption Isotherms. *J. Phys. Chem.* **1979**, *83*, 1619−1635.

DOI: 10.1021/acs.jpcb.5b11515
J. Phys. Chem. B 2016, 120, 2658−2669

(14) Eisenberg, B. Crowded Charges in Ion Channels. In *Advances in Chemical Physics*; Rice, S. A., Ed.; John Wiley & Sons, Inc.: New York, 2011; Vol. *148*, pp 77−223. Also on the arXiv at http://arxiv.org/abs/1009.1786v1001.
(15) Boda, D. Monte Carlo Simulation of Electrolyte Solutions in Biology: in and out of Equilibrium. *Annu. Rep. Comput. Chem.* **2014**, *10*, 127−164.
(16) Gillespie, D. A. Review of Steric Interactions of Ions: Why Some Theories Succeed and Others Fail to Account for Ion Size. *Microfluid. Nanofluid.* **2015**, *18*, 717−738.
(17) Berman, H. M.; Battistuz, T.; Bhat, T. N.; Bluhm, W. F.; Bourne, P. E.; Burkhardt, K.; Feng, Z.; Gilliland, G. L.; Iype, L.; Jain, S.; et al. The Protein Data Bank. *Acta Crystallogr., Sect. D: Biol. Crystallogr.* **2002**, *D58*, 899−907.
(18) Dolinsky, T. J.; Czodrowski, P.; Li, H.; Nielsen, J. E.; Jensen, J. H.; Klebe, G.; Baker, N. A. PDB2PQR: Expanding and Upgrading Automated Preparation of Biomolecular Structures for Molecular Simulations. *Nucleic Acids Res.* **2007**, *35*, W522−W525.
(19) Humphrey, W.; Dalke, A.; Schulten, K. VMD - Visual Molecular Dynamics. *J. Mol. Graphics* **1996**, *14*, 33−38.
(20) Ketchem, R. R.; Huo, W.; Cross, T. A. High-Resolution Conformation of Gramicidin A in a Lipid Bilayer by Solid-State NMR. *Science* **1993**, *261*, 1457−1460.
(21) Doyle, D. A.; Cabral, J. M.; Pfuetzner, R. A.; Kuo, A.; Gulbis, J. M.; Cohen, S. L.; Chait, B. T.; MacKinnon, R. The Structure of the Potassium Channel: Molecular Basis of K^+ Conduction and Selectivity. *Science* **1998**, *280*, 69−77.
(22) Payandeh, J.; Scheuer, T.; Zheng, N.; Catterall, W. A. The Crystal Structure of a Voltage-Gated Sodium Channel. *Nature* **2011**, *475*, 353−358.
(23) Liao, M.; Cao, E.; Julius, D.; Cheng, Y. Structure of the TRPV1 Ion Channel Determined by Electron Cryo-Microscopy. *Nature* **2013**, *504*, 107−112.
(24) Nishizawa, T.; Kita, S.; Maturana, A. D.; Furuya, N.; Hirata, K.; Kasuya, G.; Ogasawara, S.; Dohmae, N.; Iwamoto, T.; Ishitani, R.; et al. Structural Basis for the Counter-Transport Mechanism of a H +/Ca2+Exchanger. *Science* **2013**, *341*, 168−171.
(25) Santangelo, C. D. Computing Counterion Densities at Intermediate Coupling. *Phys. Rev. E* **2006**, *73*, 041512.
(26) Hilgemann, D. W. New Insights into the Molecular and Cellular Workings of the Cardiac Na /Ca2 Exchanger. *Am. J. Physiol. Cell Physiol.* **2004**, *287*, C1167−C1172.
(27) Reeves, J. P.; Hale, C. C. The Stoichiometry of the Cardiac Sodium-Calcium Exchange System. *J. Biol. Chem.* **1984**, *259*, 7733−7739.
(28) Kimura, J.; Noma, A.; Irisawa, H. Na-Ca Exchange Current in Mammalian Heart Cells. *Nature* **1986**, *319*, 596−597.
(29) Rasgado-Flores, H.; Blaustein, M. P. Na/Ca Exchange in Barnacle Muscle Cells Has a Stoichiometry of 3 Na^+/1 Ca^{2+}. *Am. J. Physiol.* **1987**, *252*, C499−C504.
(30) Hilgemann, D. W.; Nicoll, D. A.; Philipson, K. D. Charge Movement during Na^+ Translocation by Native and Cloned Cardiac Na^+/Ca^{2+}Exchanger. *Nature* **1991**, *352*, 715−718.
(31) Kang, T. M.; Hilgemann, D. W. Multiple Transport Modes of the Cardiac Na^+/Ca^{2+} Exchanger. *Nature* **2004**, *427*, 544−548.
(32) Hille, B. *Ionic Channels of Excitable Membranes*; Sinauer Associates Inc.: Sunderland, MA, 2001.

DOI: 10.1021/acs.jpcb.5b11515
J. Phys. Chem. B 2016, 120, 2658−2669